

Grace X. Gu · Markus J. Buehler

# Tunable mechanical properties through texture control of polycrystalline additively manufactured materials using adjoint-based gradient optimization

Received: 26 January 2018 / Revised: 23 May 2018  
© Springer-Verlag GmbH Austria, part of Springer Nature 2018

**Abstract** Polycrystalline materials can be characterized by the preferred orientation of grains within a material, otherwise known as texture. It has been shown that texture can affect a wide range of mechanical properties in metallic materials, including elastic moduli, yield stress, strain hardening, and fracture toughness. Recent advances in additive manufacturing of metallic materials allow for controlling the spatial variation of texture and thus provide a path forward for controlling material properties through additive manufacturing. This paper investigates the benefits, in terms of mechanical performance, of varying texture spatially. We examine the material properties of a hole in a plate under load and use an adjoint-based gradient optimization algorithm coupled with a finite element solver. The method of adjoints allows for efficient calculation of design problems in a large variable space, reducing overall computational cost. As a first step to general texture optimization, we consider the idealized case of a pure fiber texture where the homogenized properties are transversely isotropic. In this special case, the only spatially varying design variables are the angles that describe the orientation of the homogenized material at each point within the structure. Material angles for both a spatially homogeneous and a spatially heterogeneous material are optimized for quantities of interest, such as compliance and von Mises stress. Additionally, the combined effects of elasticity tensor and material orientation on optimized structures are explored, as the additive manufacturing processes can potentially vary both. This work paves a way forward to design metallic materials with tunable mechanical properties at the microstructure level and is readily adapted to other materials.

## 1 Introduction

Over the past decade, additive manufacturing has received remarkable attention and has made significant progress, especially in the case of metallic materials. Compared to traditional manufacturing methods, additive manufacturing can provide local microstructure control by tuning process parameters during different stages of manufacturing. Rather than removing material, as in traditional subtractive manufacturing, additive manufacturing of metallic materials involves layer-wise consolidation of feedstock material in the form of powder, wire, or sheet using various energy sources to form complex parts. As new feedstock materials become available, academic, industrial, and government research groups have become increasingly interested in the field of metallic additively manufactured materials and their applications [1–5]. Additive manufacturing has opened up the design space to fabricate shapes and designs that are nearly impossible to realize with other

---

G. X. Gu · M. J. Buehler (✉)

Laboratory for Atomistic and Molecular Mechanics (LAMM), Department of Civil and Environmental Engineering, Massachusetts Institute of Technology, 77 Massachusetts Ave., Cambridge, MA 02139, USA  
E-mail: mbuehler@mit.edu

G. X. Gu

Department of Mechanical Engineering, Massachusetts Institute of Technology, 77 Massachusetts Ave., Cambridge, MA 02139, USA

manufacturing methods [6–11]. With microstructure considerably affecting material properties and behavior, control of microstructure allows control of material properties, such as elastic moduli, plastic deformation, strain hardening, and fracture toughness [8, 12, 13].

Past work by several researchers has already shown that microstructure or texture control of metallic additively manufactured materials is possible using techniques such as electron beam (EBM) and directed energy deposition (DED) methods. Raghavan et al. recently used an innovative process control method that allows the operator to change melting conditions to generate a columnar or equiaxed microstructure on-demand [14]. Makiewicz et al. have used model-based process parameters with a DED technique to achieve a homogeneous microstructure with improved fatigue properties [15]. Dinda et al. reported using a laser-aided direct metal deposition process to produce texture-controlled structures on a polycrystalline substrate by adjusting the laser beam scanning velocity [16]. Dehoff et al. demonstrated the growth of highly misoriented equiaxed grains outlining the letters “D,” “O,” and “E” through the thickness of a nickel-based superalloy block comprised of columnar-oriented grains [17]. These advances on the process side of metallic additive manufacturing demonstrate the potential to optimize application-specific mechanical properties through rational control of the metal microstructure.

Texture can affect material properties, and given the progress of additive manufacturing, it is now possible to control texture. The natural next step for work in this field to take is to treat texture as a variable that can be optimized and to propose a method to achieve this goal. Optimization of materials for properties such as compliance, stiffness, thermal expansion coefficient, and fracture toughness is widespread in the literature [18–25]. Optimization methods can be divided into two broad categories: gradient-based and heuristic-based (e.g., genetic, greedy, simulated annealing). Most gradient-based methods provide a top-down approach to topology optimization focusing on macroscale structural features [9, 26]. For instance, Gaynor et al. used multi-material topology optimization to create compliant structures [19]. Buhl et al. used a gradient-based approach of Method of Moving Asymptotes (MMA) to optimize for stiffness in the structure [25]. Larsen et al. used a numerical topology optimization method to design material structures with negative Poisson’s ratio (NPR) [27]. Most optimization work for fiber-reinforced composites consists of optimizing the stacking angle of plies using genetic algorithms [23, 28, 29]. However, optimization efforts treating the microstructurally governed local spatial variability of material properties as a design variable are so far very limited, and therein lies the goal of this work.

Here, we employ an adjoint-based gradient optimization algorithm in conjunction with a finite element solver to find optimal material orientations and positions to minimize compliance and von Mises stress in a metallic additively manufactured structure. As a first step to general texture optimization, we consider the idealized case of a pure fiber texture where the homogenized properties are transversely isotropic. For this special case, the only spatially varying design variables are the angles that define the orientation of the material at each point within the structure. The method of adjoints allows for efficient calculation of this large design space problem, reducing overall computational cost. This work illustrates a novel approach to designing metallic materials that allows for tuning of mechanical properties at the microstructure level. Specifically, we present a method to optimize texture to improve material performance. The finite element modeling (model setup, boundary conditions, and material properties) and adjoint-based optimization method are described in Sect. 2. Results and discussion of simulation and optimization are presented in Sect. 3. In addition, optimizing spatial variation of material orientations for a 2D system is explored and analyzed for different objective functions. Conclusions and future outlook are discussed in Sect. 4.

## 2 Methods

Spatially optimal material orientations of an additively manufactured (AM) structure are obtained using a finite element solver combined with an optimization software. COMSOL Multiphysics [30] is used for both optimization and structural finite element analysis. This software can incorporate adjoints in its optimization subroutines to efficiently solve problems. Here we consider a hole in a plate where the hole represents a structural feature that gives rise to a stress concentration. The objectives of the proposed optimization are to minimize the maximum stress point near the hole and to minimize the overall compliance of the structure. The methods used here can be extended to study problems in linear elastic fracture mechanics (LEFM), where cracks are also characterized as stress concentrators in structures.

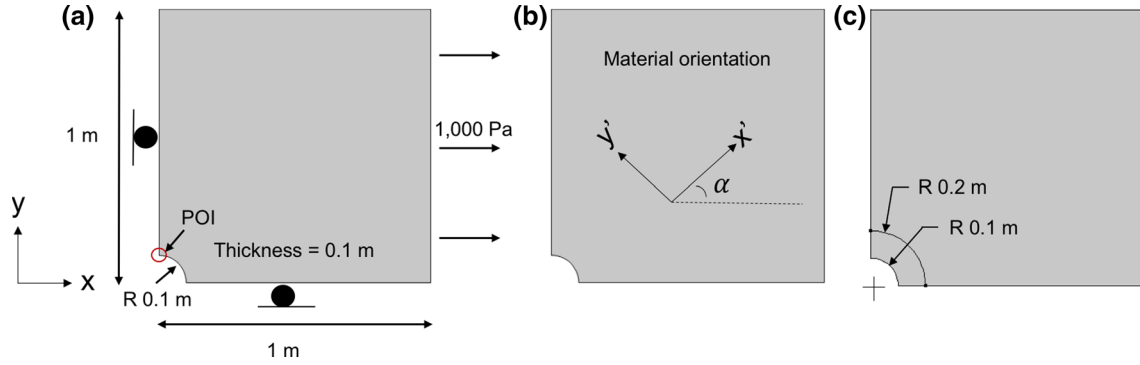


**Fig. 1** Model inputs. **a** Quarter geometry with dimensions, leveraging system symmetry, and the configuration of the uniaxial tension with a boundary distributed stress of 1000 Pa is shown. The point of interest (POI) at which maximum stress occurs in suboptimal cases under these loading conditions is also indicated. **b** Local material coordinate system  $x' - y'$  as related to the global coordinate system  $x - y$  through rotation angle  $\alpha$ . **c** Annulus domain used for variations of von Mises objective functions

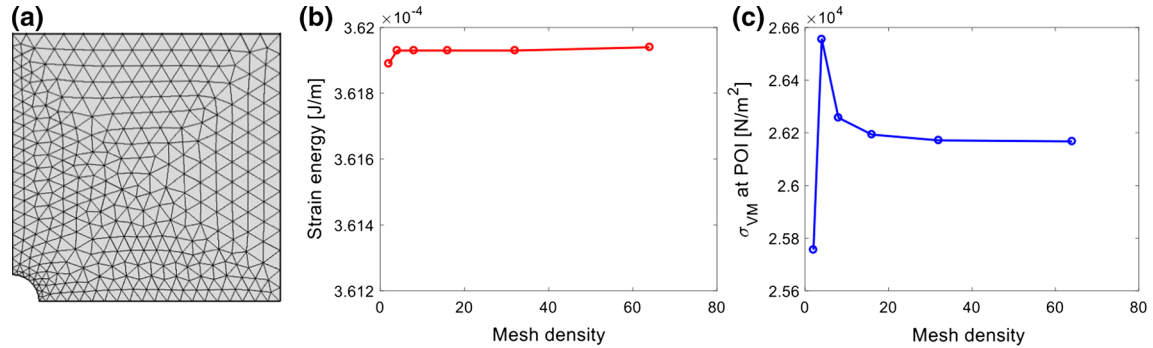


**Fig. 2** Finite element analysis **a** Mesh used for the finite element analysis. **b, c** Mesh convergence study for the two objective functions of strain energy and von Mises stress at the point of interest (POI)

## 2.1 Finite element analysis

### 2.1.1 Model setup and boundary conditions

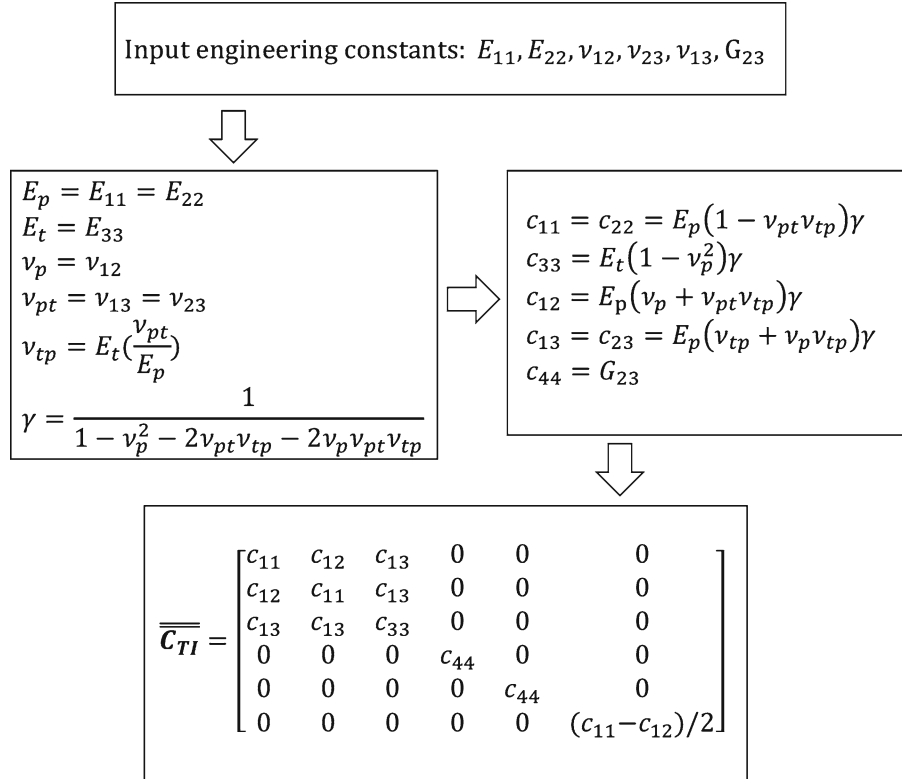
The model problem studied in this work is a two-dimensional hole in a plate with dimensions shown in Figs. 1a, b. The plate is assumed to be under plane stress conditions as the through thickness is small compared to the other dimensions. A distributed normal stress of 1000 Pa is applied at the edge of the sample at  $x = 1$  m. Symmetry boundary conditions are imposed on the surfaces at  $x = 0$  and  $y = 0$ . This is imposed to make use of the biaxial symmetry of the material, requiring only a quarter of the structure to be analyzed. The edge at  $y = 1$  m is left unconstrained. Figure 1c shows the annulus domain used for variations of von Mises objective functions, used in Sect. 3.5. The mesh, shown in Fig. 2, is chosen for optimal computational efficiency; a mesh convergence study is conducted and shown in Fig. 2. Mesh density is the number of elements along surfaces of  $x = 0$  and  $y = 0$ . A linear elastic material model is assumed throughout this work.

### 2.1.2 Material properties

The material considered here is an AM 304L stainless steel. Material properties for the model considered in this paper are taken from reference [31]. In their work, the granular material was homogenized using a method that employed a geometry that respected the grain distribution and directionality of the fibers. Properties of austenite were assigned to the grains. Unit loads in each of the three orthogonal directions were applied to obtain bulk representative volume element (RVE) properties for the transverse stiffness values. The material properties are chosen from reference [31] because the studied material,  $\langle 100 \rangle$  fibers of austenite, has been observed experimentally in AM processes and is relevant to the work presented here. The material properties are sampled with zero spatial correlations. For comparison, we also consider a set of homogenized isotropic

**Table 1** Homogenized material properties. Tabulated are the elastic moduli, Poisson's ratios, and shear moduli for the isotropic and transversely isotropic pure fiber texture cases from reference [31]

	Elastic modulus (GPa)			Poisson's ratio (-)			Shear modulus (GPa)		
	$E_{11}$	$E_{22}$	$E_{33}$	$\nu_{12}$	$\nu_{23}$	$\nu_{13}$	$G_{12}$	$G_{23}$	$G_{13}$
Isotropic	198	198	198	0.29	0.29	0.29	76.5	76.5	76.5
Pure fiber texture	143	143	90.9	0.11	0.62	0.62	58	126	126

**Fig. 3**  $\overline{\overline{\mathbf{C}}}_{TI}$  calculation for a transversely isotropic material

material properties obtained from an RVE with randomly oriented equiaxed grains (no preferred orientation and no texture). Both sets of material parameters are reported in Table 1.

The material coordinate system is shown in Fig. 1b, where  $\alpha$  is the angle between the material coordinate system  $x', y'$  and the global coordinate system  $x, y$ . Three optimization cases are studied:

1.  $\alpha$  is varied in a spatially homogeneous material
2.  $\alpha$  is varied in a spatially heterogeneous material
3.  $\alpha$  and  $p$  are varied in a spatially heterogeneous material

where  $p$  is an indicator function with values between 0 and 1 that varies the degree of transverse isotropy in the material elasticity tensor. The parameter  $p$  represents the weighting of transverse to isotropic properties in the elasticity tensor. This parameter is varied during the optimization procedure. In effect,  $\overline{\overline{\mathbf{C}}}$  is an elasticity tensor that takes on more transverse properties by varying  $p$  from 0 to 1. At a material point, for  $p = 1$ , the elasticity tensor  $\overline{\overline{\mathbf{C}}}$  corresponds to the elasticity tensor of a transversely isotropic material,  $\overline{\overline{\mathbf{C}}}_{TI}$ , while for  $p = 0$ , we recover the isotropic elasticity tensor,  $\overline{\overline{\mathbf{C}}}_I$ :

$$\overline{\overline{\mathbf{C}}} = p\overline{\overline{\mathbf{C}}}_{TI} + (1 - p)\overline{\overline{\mathbf{C}}}_I. \quad (1)$$

$\overline{\overline{\mathbf{C}}}_{TI}$  and  $\overline{\overline{\mathbf{C}}}_I$  are defined by the elastic properties given in Table 1.  $\overline{\overline{\mathbf{C}}}_{TI}$  is described in Fig. 3 for a transversely isotropic material [32].  $\overline{\overline{\mathbf{C}}}_I$  is the completely isotropic version of  $\overline{\overline{\mathbf{C}}}_{TI}$ . Note that this is a simplified way to vary

the elastic properties. A more rigorous approach would be to allow the texture to vary from “none” to “pure fiber” and then rerun an RVE simulation to recover the homogenized elastic constants. This would involve doing this for several “ $p$ ” values and then fitting an interpolation curve to each elastic constant so that it can be used by COMSOL, which is an interesting extension of this work.

## 2.2 Optimization

### 2.2.1 Objective functions

Two main objective functions are explored in this study. The first is the strain energy ( $Q_1$ ), which is defined as the integral of strain energy density ( $W_S$ ) over the entire domain. Strain energy balances the work done by the applied load. As a result, minimizing strain energy minimizes the displacement induced at the points where load is applied, effectively minimizing the compliance of the structure and maximizing its stiffness. The second objective function studied is the von Mises stress ( $Q_2$ ) at the point of interest (POI), which is the location of maximum stress around the hole for a general isotropic material. The idea behind the second objective function is to find a solution which will have a minimum value of stress at a critical point in the system, which is the maximum stress point. The functional forms for  $Q_1$  and  $Q_2$  are given by

$$\begin{aligned} Q_1 &= \int_{\Omega} W_S d\Omega, \\ Q_2 &= \sigma_{VM}|_{\text{POI}}. \end{aligned} \quad (2)$$

The local orientation of the material coordinate system,  $\alpha$ , is varied in this problem as defined in Sect. 2.1.2.

### 2.2.2 The adjoint-based gradient method

To optimize our system, we use the gradient-based method of Method of Moving Asymptotes (MMA) from the COMSOL optimization toolbox. This is an iterative procedure that generates and solves a convex sub-problem within each iteration, which is suitable for our optimization problem [33]. Upper and lower moving asymptotes are calculated to adjust the curvature of the approximate functions, with the selection of the moving asymptotes being largely heuristic. The adjoint method is a numerical method for efficiently computing the gradient of a function or operator with respect to a large number of design variables [30,34]. The adjoint orients the gradient of a function toward its parameters, yielding a constrained optimization formulation. Additionally, adjoint methods can efficiently solve for elements of  $\alpha$  and  $p$ , whose elements map to different spatial points and can vary within the structure. Utilizing this method also means that calculating the inverse stiffness matrix can be avoided, drastically reducing the total computational overhead. The optimization problem requires:

$$\frac{dQ}{d\alpha} = 0, \quad (3)$$

where  $Q$  is the objective function and  $\alpha$  is the vector of design variables in the optimization problem. In this study, the objective functions and design variables are defined in Eq. (2) and Fig. 1, respectively. Applying the chain rule to Eq. (3), the optimization condition becomes

$$\frac{dQ}{d\alpha} = \frac{dQ}{du} \frac{du}{d\alpha}, \quad (4)$$

where  $u$  is the displacement vector. Now, we introduce an adjoint variable defined as

$$\lambda^T = \frac{dQ}{du} \overline{\overline{\mathbf{K}}}^{-1}(\alpha) \rightarrow \frac{dQ}{d\alpha} = \lambda^T \overline{\overline{\mathbf{K}}}(\alpha), \quad (5)$$

where  $\lambda$  is the list of adjoint variables and  $\overline{\overline{\mathbf{K}}}$  is the stiffness matrix. We now need to solve for  $\frac{du}{d\alpha}$  from

$$\overline{\overline{\mathbf{K}}}(\alpha) u = F, \quad (6)$$

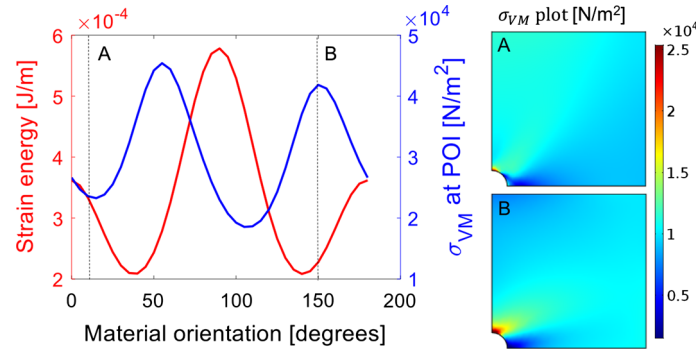


**Fig. 4** Parametric sweep of spatial homogeneous material orientations. Strain energy and von Mises stress vary with material orientations. Cases A and B are depicted in the graph on the left. Von Mises stress plots for cases A ( $\alpha = 15^\circ$ ) and B ( $\alpha = 150^\circ$ ), shown on the right, depict differences in stress contours as a function of sample orientation

where  $F$  is the vector of applied forces acting on the system. Differentiating Eq. (6) yields

$$\bar{\bar{\mathbf{K}}}(\alpha) \frac{d\mathbf{u}}{d\alpha} + \frac{d\bar{\bar{\mathbf{K}}}(\alpha)}{d\alpha} \mathbf{u} = \frac{d\mathbf{F}}{d\alpha} = 0. \quad (7)$$

This means that

$$\frac{d\mathbf{u}}{d\alpha} = -\bar{\bar{\mathbf{K}}}(\alpha)^{-1} \frac{d\bar{\bar{\mathbf{K}}}(\alpha)}{d\alpha} \mathbf{u}. \quad (8)$$

Now, the components from Eqs. (5) and (8) can be combined into Eq. (4) to result in

$$\frac{dQ}{d\alpha} = \frac{dQ}{d\mathbf{u}} \frac{d\mathbf{u}}{d\alpha} = \left( \lambda^T \bar{\bar{\mathbf{K}}}(\alpha) \right) \left( -\bar{\bar{\mathbf{K}}}(\alpha)^{-1} \frac{d\bar{\bar{\mathbf{K}}}(\alpha)}{d\alpha} \mathbf{u} \right) = -\lambda^T \frac{d\bar{\bar{\mathbf{K}}}(\alpha)}{d\alpha} \mathbf{u}. \quad (9)$$

The method of adjoints outlined here can be used to solve for spatially varying material orientations. The adjoint method eliminates the inverse stiffness matrix ( $\bar{\bar{\mathbf{K}}}^{-1}$ ) from the calculation, hence reducing the computational cost.

### 3 Results and discussion

#### 3.1 Parametric sweep

A parametric sweep of various material angles ( $\alpha$ ) is performed to discern the effects of material orientation on mechanical properties. The same angle is assumed for all positions in the structure and a forward analysis (with no optimization involved) of various material orientations is executed. For the case of a spatially homogeneous material,  $\alpha$  is a vector of identical elements, which for clarity will be denoted by the single scalar value,  $\alpha$ . Results are shown in Fig. 4. Both strain energy ( $Q_1$  from Eq. 2) and von Mises stress ( $Q_2$  from Eq. 2) vary with material orientation under the same load. The curve for strain energy is perfectly symmetric, while the curve for von Mises stress at the selected point of interest is not. The reason for this is that the equation for solving strain energy is an integral over the entire material domain, while the von Mises stress objective is taken at a single point. This identification of symmetry is critical for the optimization step and sets different angle constraints for the two objective functions. As a result, for strain energy, the angles are constrained from  $0^\circ$  to  $90^\circ$ , while for von Mises, the angles are constrained from  $0^\circ$  to  $180^\circ$ . Additionally, for both properties,  $\alpha = 0^\circ$  and  $\alpha = 180^\circ$  recover the same answer, which is true because they are equidistant from the same symmetry axis. Two cases on the von Mises curve are compared, A and B, with  $\alpha = 15^\circ$  at A and  $\alpha = 150^\circ$  at B. The von Mises stress plots for the two different points are very different for the two angles, as shown in Fig. 4. At point B, there is higher stress and a larger stress concentration around the hole compared to point A. This parametric sweep of the forward analysis shows that material orientation has a significant effect on the objective functions.

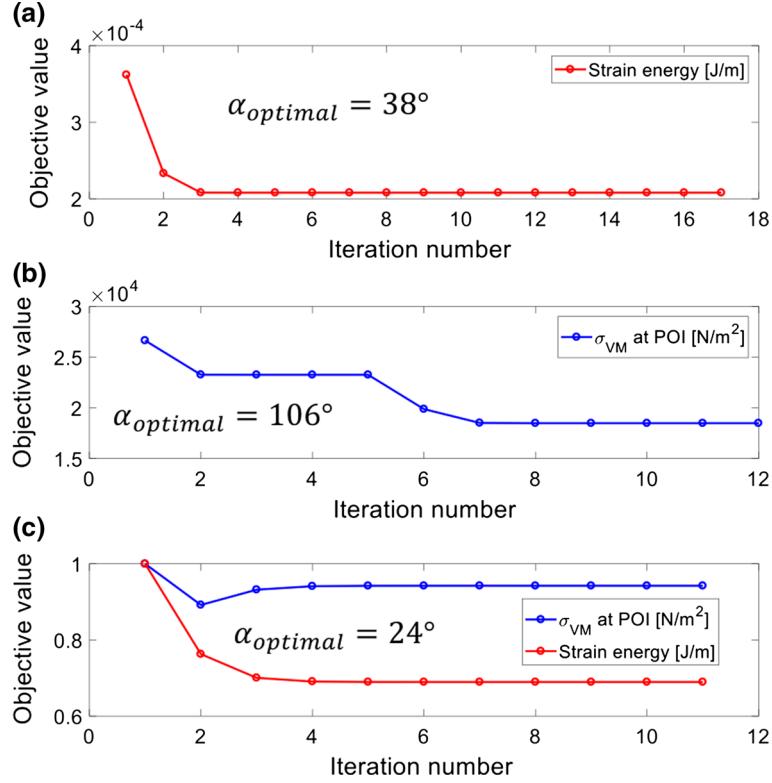


**Fig. 5** Optimization with spatially homogeneous properties. Objective value as a function of iteration number in the simulation is shown for **a** strain energy, **b** von Mises stress at POI, and **c** both strain energy and von Mises stress at POI (multi-objective optimization using equal weighting). Optimal angles for all three scenarios are shown in the respective plots

### 3.2 Optimization with spatially homogeneous properties

Next, we perform an optimization study to determine the optimal material orientation for a structure with spatially homogeneous properties and constant material stiffness. For the first objective function of strain energy,  $\alpha$  is constrained from  $0^\circ$  to  $90^\circ$  due to the symmetry in the parametric sweep. Here, just as in the parametric sweep,  $\alpha$  is a vector of all the same values, which for clarity will just be denoted with one scalar value,  $\alpha$ . From the parametric sweep, the minimum point of  $Q_1$  is around  $\alpha = 40^\circ$  (Fig. 4). After optimization, starting with an initial point of  $\alpha = 0^\circ$ , we discover that the optimal angle is  $\alpha = 38^\circ$ . This helps to verify that the optimization method is working correctly and agrees with the results of our forward analysis. Figure 5 shows the objective value of strain energy decreasing with each iteration and eventually converging to a solution. For the second objective of von Mises stress,  $\alpha$  is constrained from  $0^\circ$  to  $180^\circ$ . From the parametric sweep, the minimal point is around  $105^\circ$ . Figure 5 shows the objective value decreasing with each iteration and eventually converging to a solution of  $\alpha = 106^\circ$ . This provides yet another validation of the optimization routine.

In addition to optimizing these two objectives separately, multi-objective optimization can be considered for applications that need to have optimal values for both objectives. To do multi-objective optimization we use a sum of the objectives (with equal weighting),  $Q = Q_1 + Q_2$ . The properties are first normalized to prevent any bias from the magnitude of the properties with different units using solutions from  $\alpha = 0^\circ$ . Figure 5 shows the objective value after each iteration for both properties. In the beginning, both properties decrease; however, at some point, the objective function for von Mises stress increases to allow for even more decrease in strain energy, which consistently decreases with each iteration. This behavior reveals the tradeoffs necessary to find an optimal value that is most beneficial to the system. The optimal angle for the multi-objective problem with equal weighting is  $\alpha = 24^\circ$ . It is important to note that for different applications, this equal weighting can be adjusted to suit a certain application that may require better performance in one of the objectives.

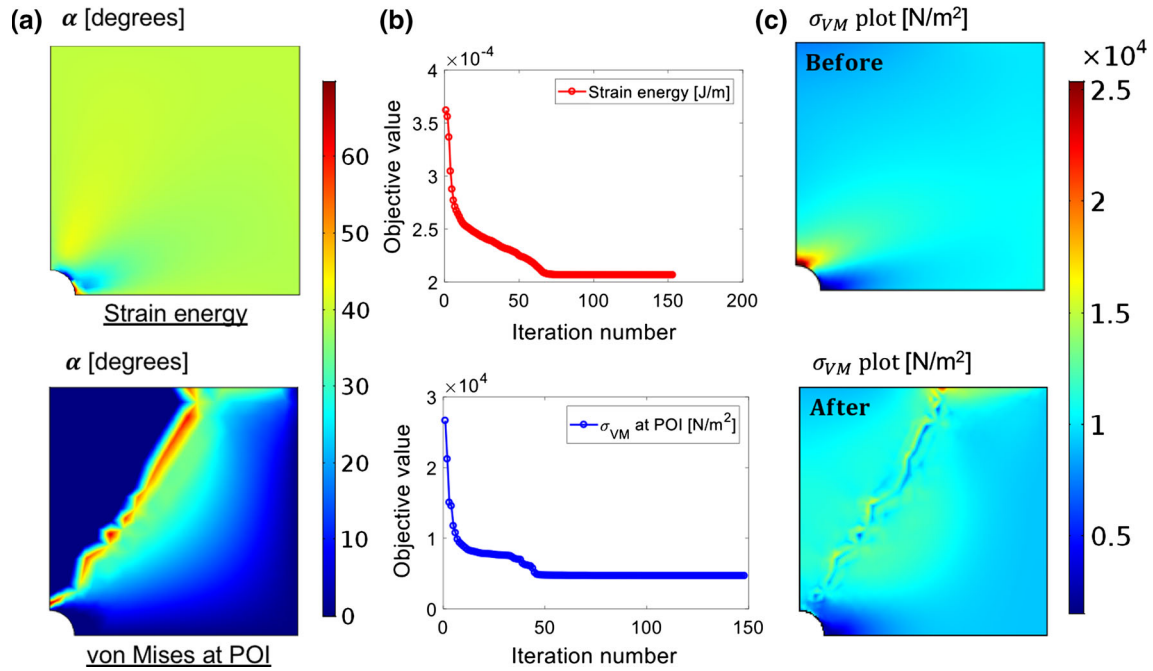


**Fig. 6** Optimization with spatially heterogeneous properties. **a** Spatially varying optimal angle is shown for strain energy and von Mises stress at POI. **b** Objective value as a function of iteration number is minimized and converged for strain energy and von Mises at POI. **c** Before and after optimization von Mises stress plots optimized to minimize von Mises stress at POI show much lower stress after optimization

### 3.3 Optimization with spatially heterogeneous properties

The previous section discussed an optimal material angle for the entire sample with spatially uniform material properties. However, allowing the material orientation angle to vary spatially can better leverage the evolving capability of additive manufacturing to produce point-wise material control within a printed structure. Using the method of adjoints allows us to efficiently solve for optimal angles at each point in the geometry (Sect. 2). For the strain energy objective function, Fig. 6 shows a color plot of the optimal angles in degrees. Most parts of the geometry, far away from the hole area, are in the regime of  $\alpha = 40^\circ$ , which is very close to the optimal angle obtained from the optimization of spatially homogeneous properties of  $\alpha = 38^\circ$ . Near the hole, the angles seem to vary much more to decrease the strain energy of the system and mitigate the effects of the hole. Also shown in Fig. 6 is the strain energy objective value decreasing with each iteration and eventually converging to a minimum value.

For the von Mises objective function, Fig. 6 shows a color plot of the optimal angles. It can be seen that near the POI, the optimal angles start to deviate along the maximum shear stress line, which is at a 45-degree angle from the hole. This is done in order to lower the stress at the POI. Additionally, the von Mises stress plot *before* optimization is shown for  $\alpha = 150^\circ$ , compared to the von Mises stress plot with optimal angles *after* optimization (heterogeneous material orientation case). With optimization, most of the stress that was near the hole is dissipated and the stress is much more distributed in the material, diminishing the effects of the hole.

### 3.4 Optimization with variable elastic properties

The two previous studies have assumed constant stiffness properties; however, the AM process potentially offers the capability to vary both stiffness properties and material orientation throughout a printed structure. Thus, another variable is added to consider material variation in the system. We introduce the variable  $p$  to consider the degree of isotropy of the stiffness matrix (Eq. (1)). When  $p = 0$ , the material is completely isotropic, and when  $p = 1$ , the material is transversely isotropic, recovering the case of a pure fiber texture. Intermediate values of  $p$  correspond to intermediate materials between these two extremes. Therefore, for this optimization problem, there are two variables that vary spatially,  $\alpha$  and  $p$ .

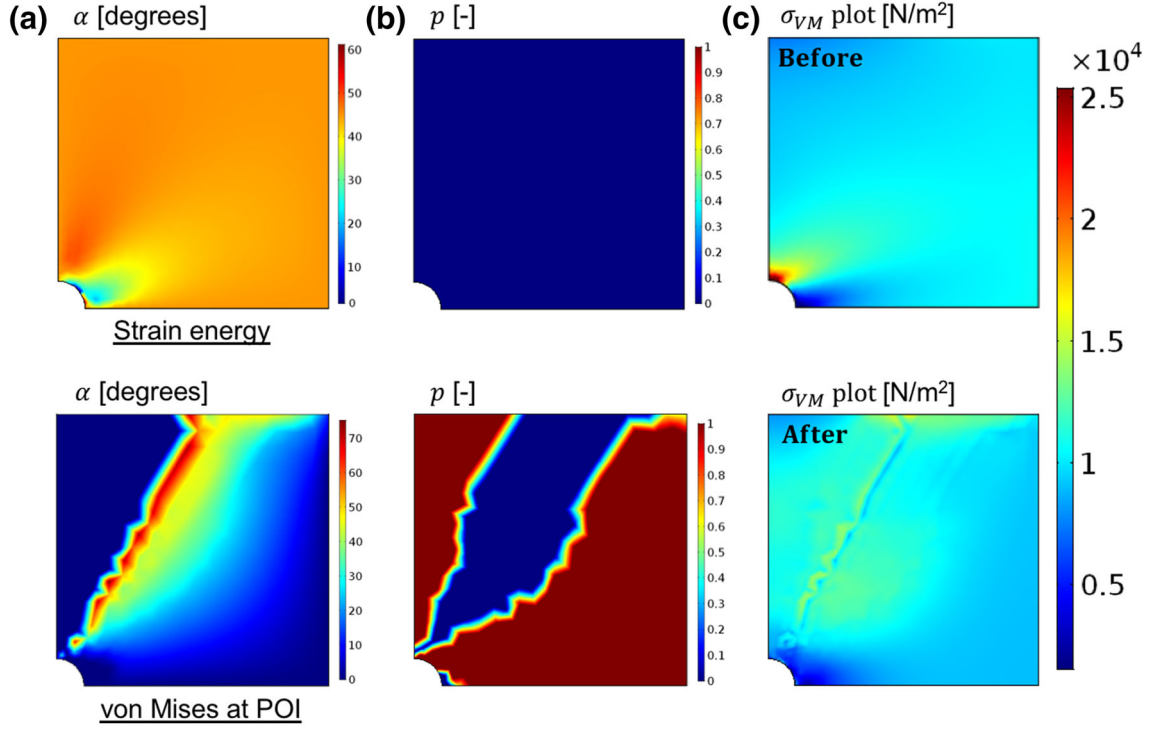


**Fig. 7** Optimization of variable elastic properties. Spatially variable optimal **a** angles  $\alpha$  and indicator function, **b**  $p$  (degree of isotropy discussed in Sect. 2) are shown for the objective function of strain energy (top) and von Mises stress at POI (bottom). **c** Plots show von Mises stress before (top) and after (bottom) optimization to minimize von Mises stress at the POI

For the strain energy objective function,  $\alpha$  and  $p$  values are shown in Fig. 7; the plot is similar to the previous spatially heterogeneous properties plot. Although  $p$  can vary spatially, the optimal value is  $p = 0$  everywhere in the geometry, meaning it recovers the isotropic solution. Since strain energy is correlated to stiffness and the isotropic solution has high values for elastic modulus in most of the directions, this solution makes intuitive sense. For the von Mises objective, the solution for angles is quite similar to that in Sect. 3.3. The variation in  $p$  also lies around the 45-degree angle between the hole and the edge of the plate. The von Mises stress plot shows more dissipated stress away from the hole where maximum stress was originally located.

### 3.5 Variations of von Mises objective function

In the previous section, the von Mises objective function is solved for at a specific point. This method works in applications where it is necessary to mitigate the stress at a point. However, in some applications, an average stress over a domain is more important. Here, we studied two additional cases, an averaged von Mises stress over the entire domain and an averaged von Mises stress over an annulus with radius 0.1 m around the hole (shown in Fig. 1c).

The objective function for the entire domain is chosen to be the integral of the squared von Mises stress over the geometry ( $T_{VM}$ ):

$$T_{VM} = \int_{\Omega} \sigma_{VM}^2 d\Omega, \quad (10)$$

where  $\sigma_{VM}$  is the von Mises stress at each point in the geometry. To calculate the von Mises stress proxy, we integrate the square of the von Mises stress over the geometry. The square of the von Mises stress is chosen to accentuate the features of interest. The results are shown in Fig. 8a. For this objective function, the band of angles along the 45-degree line between the hole and plate edge no longer appear; the same applies for the variable  $p$ . Looking at the von Mises stress plot, there still exists very high stress around the hole, meaning that the stress is not successfully mitigated. Additionally, with each subsequent iteration, the objective value

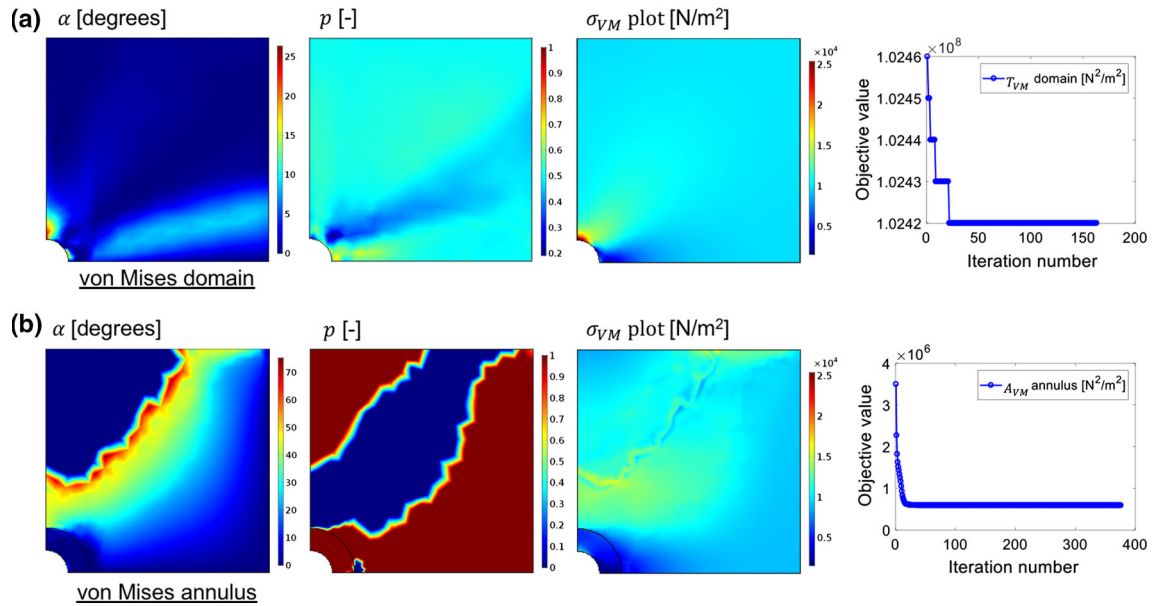


**Fig. 8** Varying objective functions for von Mises stress. From left to right: Optimal angles,  $\alpha$ , indicator function,  $p$  (degree of isotropy discussed in Sect. 2), resulting von Mises stress plot, and objective value with iteration number, is shown for the objective function of integrating the square of von Mises stress **a** over the entire domain ( $T_{VM}$ ) and **b** over an annulus around the hole ( $A_{VM}$ )

does not decrease much for this objective function. From this analysis, it seems the angle effects cancel each other out when integrating over the entire domain rather than a region of interest.

For the von Mises stress around an annulus, we integrate the square of von Mises stress over a region one radius value larger than the radius of the hole ( $A_{VM}$ ):

$$A_{VM} = \int_{r_1}^{r_2} \sigma_{VM}^2 d\Omega, \quad (11)$$

where  $r_1$  and  $r_2$  are the inner and outer radii of the annulus. Results for this objective function are shown in Fig. 8b. When optimizing around an annulus, the angle profile is shifted from before, when von Mises stress was defined at a point. This method helps to shift the stress away from the *region* of interest as opposed to only the *point* of interest. It can also be seen that with each iteration, the objective value is decreasing, and, from the von Mises stress profile, the high stress values near the region of interest disappear. The various methods to solve for the von Mises objective function can be modified, such as the annulus size and shape, depending on the application.

#### 4 Conclusions and future work

In this work, a technique to optimize material orientations of polycrystalline materials using a combination of finite element analysis and gradient-based optimization is presented. To efficiently solve for the optimal material orientations, an adjoint-based optimization method is used. Material angles for spatially homogeneous and heterogeneous materials are optimized for quantities of interest, such as compliance and von Mises stress. Additionally, the combined effects of stiffness tensor and material orientation variables on optimized structures are explored, as the AM processes potentially offer the capability to vary both. The methods and framework presented here can be extended to study other structures and designs and offer a tool to create optimized geometries with varying material orientations. Here, we consider a linear elastic model and optimize behavior in the small-strain regime. An expansion of this work could be to extend the approach to explore:

- nonlinear behavior, such as plasticity;
- dynamic high-strain rate analysis; and
- three-dimensional analysis with three Euler angles as variables.

Another extension could be to combine material orientation with topology optimization, which would involve four variables: the three Euler angles and material density (indicating whether there is material there or void). This work demonstrates the possibility to tune mechanical properties at the microstructure level of metallic materials and can be applied to other materials as well.

**Acknowledgements** The authors would like to acknowledge Sandia National Labs for supporting this research. The authors would also like to thank Judy Brown, Joseph Bishop, and Eliot Fang for their immensely helpful discussions. Additionally, the authors would like to thank Sam Raymond and Maysam Bandpay for their insightful discussions. Authors also appreciate support from the NDSEG Fellowship.

## References

- Gibson, I., Rosen, D., Stucker, B.: Additive Manufacturing Technologies: Design for additive manufacturing. Springer, Boston, MA (2010)
- Gibson, I., Rosen, D.W., Stucker, B.: Additive Manufacturing Technologies. Springer, Berlin (2010)
- Goehrke, S.A.: Metal 3D Printing with Machine Learning: GE Tells Us About Smarter Additive Manufacturing. <https://3dprint.com/191973/3d-printing-machine-learning-ge/> (2017)
- Murr, L.E., Martinez, E., Amato, K.N., Gaytan, S.M., Hernandez, J., Ramirez, D.A., Shindo, P.W., Medina, F., Wicker, R.B.: Fabrication of metal and alloy components by additive manufacturing: examples of 3D materials science. *J. Mater. Res. Technol.* **1**(1), 42–54 (2012)
- Gorji, M.B., Tancogne-Dejean, T., Mohr, D.: Heterogeneous random medium plasticity and fracture model of additively-manufactured Ti-6Al-4V. *Acta Materialia* **148**, 442–455 (2018)
- Compton, B.G., Lewis, J.A.: 3D-printing of lightweight cellular composites. *Adv. Mater.* **26**(34), 5930–5935 (2014)
- Gu, G.X., Takaffoli, M., Buehler, M.J.: Hierarchically enhanced impact resistance of bioinspired composites. *Adv. Mater.* **29**(28), 1700060 (2017)
- Jared, B.H., Aguilo, M.A., Beghini, L.L., Boyce, B.L., Clark, B.W., Cook, A., Kaehr, B.J., Robbins, J.: Additive manufacturing: toward holistic design. *Scr. Mater.* **135**, 141–147 (2017)
- Zegard, T., Paulino, G.H.: Bridging topology optimization and additive manufacturing. *Struct. Multidiscip. Optim.* **53**(1), 175–192 (2016)
- Gu, G.X., Libonati, F., Wettermark, S., Buehler, M.J.: Printing nature: unraveling the role of nacre’s mineral bridges. *J. Mech. Behav. Biomed. Mater.* **76**, 135–144 (2017)
- Gu, G.X., Su, I., Sharma, S., Voros, J.L., Qin, Z., Buehler, M.J.: Three-dimensional-printing of bio-inspired composites. *J. Biomech. Eng.* **138**(2), 021006 (2016)
- Das, S., Bourell, D.L., Babu, S.: Metallic materials for 3D printing. *MRS Bull.* **41**(10), 729–741 (2016)
- Ding, Y., Muñiz-Lerma, J., Trask, M., Chou, S., Walker, A., Brochu, M.: Microstructure and mechanical property considerations in additive manufacturing of aluminum alloys. *MRS Bull.* **41**(10), 745–751 (2016)
- Raghavan, N., Dehoff, R., Pannala, S., Simunovic, S., Kirka, M., Turner, J., Carlson, N., Babu, S.S.: Numerical modeling of heat-transfer and the influence of process parameters on tailoring the grain morphology of IN718 in electron beam additive manufacturing. *Acta Mater.* **112**, 303–314 (2016)
- Makiewicz, K., Babu, S., Keller, M., Chaudhary, A.: Microstructure evolution during laser additive manufacturing of Ti6Al4V Alloys. In: Proceedings of International Conference on Trends in Welding Research, Chicago, IL (2012)
- Dinda, G., Dasgupta, A., Mazumder, J.: Texture control during laser deposition of nickel-based superalloy. *Scr. Mater.* **67**(5), 503–506 (2012)
- Dehoff, R., Kirka, M., Sames, W., Bilheux, H., Tremsin, A., Lowe, L., Babu, S.: Site specific control of crystallographic grain orientation through electron beam additive manufacturing. *Mater. Sci. Technol.* **31**(8), 931–938 (2015)
- Brackett, D., Ashcroft, I., Hague, R.: Topology optimization for additive manufacturing. In: Proceedings of the Solid Freeform Fabrication Symposium, Austin, TX, USA, pp. 348–362 (2011)
- Gaynor, A.T., Meisel, N.A., Williams, C.B., Guest, J.K.: Multiple-material topology optimization of compliant mechanisms created via PolyJet three-dimensional printing. *J. Manuf. Sci. Eng.* **136**(6), 061015 (2014)
- Gu, G.X., Chen, C.-T., Buehler, M.J.: De novo composite design based on machine learning algorithm. *Extreme Mech. Lett.* **18**, 19–28 (2017)
- Gu, G.X., Dimas, L., Qin, Z., Buehler, M.J.: Optimization of composite fracture properties: method, validation, and applications. *J. Appl. Mech.* **83**(7), 071006 (2016)
- Gu, G.X., Wettermark, S., Buehler, M.J.: Algorithm-driven design of fracture resistant composite materials realized through additive manufacturing. *Addit. Manuf.* **17**, 47–54 (2017)
- Soremekun, G., Gürdal, Z., Haftka, R., Watson, L.: Composite laminate design optimization by genetic algorithm with generalized elitist selection. *Comput. Struct.* **79**(2), 131–143 (2001)
- Bendsøe, M.P., Sigmund, O., Bendsøe, M.P., Sigmund, O.: Topology Optimization by Distribution of Isotropic Material. Springer, Berlin (2004)
- Buhl, T., Pedersen, C.B., Sigmund, O.: Stiffness design of geometrically nonlinear structures using topology optimization. *Struct. Multidiscip. Optim.* **19**(2), 93–104 (2000)
- Eschenauer, H.A., Olhoff, N.: Topology optimization of continuum structures: a review. *Appl. Mech. Rev.* **54**(4), 331–390 (2001)
- Larsen, U.D., Sigmund, O., Bouwst, S.: Design and fabrication of compliant micromechanisms and structures with negative Poisson’s ratio. *J. Microelectromech. Syst.* **6**(2), 99–106 (1997)

28. Le Riche, R., Haftka, R.T.: Optimization of laminate stacking sequence for buckling load maximization by genetic algorithm. *AIAA J.* **31**(5), 951–956 (1993)
29. Lin, C.-C., Lee, Y.-J.: Stacking sequence optimization of laminated composite structures using genetic algorithm with local improvement. *Compos. Struct.* **63**(3), 339–345 (2004)
30. Multiphysics, C.O.M.S.O.L.: Modeling Software, User Manual (2016)
31. Brown, J.A., Bishop, J.E.: Quantifying the impact of material-model error on macroscale quantities-of-interest using multi-scale a posteriori error-estimation techniques. *MRS Adv.* **1**(40), 2789–2794 (2016)
32. Bower, A.F.: Constitutive models: relations between stress and strain, chap. 3. In: *Applied Mechanics of Solids*, pp. 91–93 (2009)
33. Svanberg, K.: The method of moving asymptotes—a new method for structural optimization. *Int. J. Numer. Methods Eng.* **24**(2), 359–373 (1987)
34. Choi, K.K., Kim, N.-H.: *Structural Sensitivity Analysis and Optimization 1: Linear Systems*. Springer, New York (2006)

**Publisher's Note** Springer Nature remains neutral with regard to jurisdictional claims in published maps and institutional affiliations.